International Journal of Science and Research (IJSR)
ISSN (Online): 2319-7064
Index Copernicus Value (2015): 78.96 | Impact Factor (2015): 6.391

Experimental and Simulation Study of Laser Hole Drilling in Stainless Steel Using Pulsed Nd:YAG Laser

Mohammed A. Hussain

Department of Laser and Optoelectronics Engineering, Alnahrain University, Baghdad

Abstract: ***This work presents an experimental and simulation study of percussion laser hole drilling in 1.2mm thick sheet of AISI304 stainless steel. Drilling experiments using Nd:YAGlaser pulses of 1.0 to 7.0ms duration, 0.35 to 2.5J energy as single shots, in addition to a series of 10 pulses of 1msduration at 10 pulse repetition frequency (prf) have been performed in ambient air.The experimental results have been used for the comparison with the simulationresults. COMSOL Multiphysics 5.1 software has been employed to simulate the heating cycles of the 10prf shots, and the 5.0mssingle shot. The simulation has been performed in terms of 2D-Axisymmetric, comprising the heat transfer differential equations, phase change to liquid and vapour, laminar fluid flow, adaptive mesh refinement, convection and radiation losses, in addition to heat source propagation velocity. The cooling cycles following pulse extinguishment, using formulated initial thermal condition, have been simulated also for two samples from the 10prf sequence(after the 4^{th} and the 9^{th} pulse),and for the 5.0ms shot.Simulation showed that full cooling occurs within a few tens of milliseconds,and no residual heat would be carried forward to the subsequent heating pulse when operating with low pulse repetition rate.***

Keywords: Laser hole drilling, stainless steel, COMSOL simulation, heating and cooling simulation

1. Introduction

A wide range of materials have been drilledusing different types of lasers since the invention of the first ever laser i.e. the Ruby laser. This is being motivated by the precision of hole geometry and material removal rate which is enhanced by melt expulsion from the hole crater [1]-[4]. Laser drilling in metallic, nonmetallic, and semiconductors has been experimented, applied and studied using either percussion or trepanning techniques, utilizing long, short, and ultra-short laser pulses. Laser hole drilling researcheshave been focused onto the performance of material removal and equally on the produced hole quality features, by studying and controlling the process parameters such as; pulse energy, pulse duration, power intensity, pulse shape and pulse repetition rate [5]-[10].

Various Stainless steel alloys have been used in diverse applications ranging from house hold utensils to aerospace and atomic energy industries. These alloys are being employed primarily as corrosion resistance, highstrengthand quite often as heat resisting metals. AISI 304 (or so-called 18/8) alloy is the most common amongst the variety of stainless steel types, this is due to its wide spectrum of applications of this alloy.

The initiation and evolution of holes drilled by laser radiation are achieved by two major mechanisms, vaporization and melt expulsion by the induced reaction of the vapour pressure.This fact has been confirmed by almost all of the reviewed literature and by the experimental observations of the present work. The proportion of material removal by either mechanism is a function of the process parameters settings, i.e. laser pulse parameters, and of the physical and thermal material properties. One general rule can be concluded so far, that is the shorter pulse duration (i.e. the higher power intensity by default), the more material proportion removed as vapour, this may also lead toimproved quality of hole geometry [4], [8], [9],[11], [12], [13], [14].

Laser hole drilling studies in stainless have been conducted in many researches.For instance,the authors of reference [12] had analyzed the repeatability of laser percussion drilling using Nd:YAG laser in 2 mm thick stainless-steel sheets. They found thatthe characteristic of melt ejection is dependent on the setting of the process parameters, and is having a significant influence on entrance hole geometry and hence repeatability.

Brajdic et.al. [13] hadperformed deep drilling of 5, 8 and 10mm stainless steel plates, usingtwo, simultauously operating, pulsed Nd:YAG lasersone ewith pulse duration of 0.5ms superposed by 17ns pulses from the other. Enhanced drilling speed and better reproducibility of the drilling time were related to the formation of modified closures in the hole during percussion drilling, and to the intensity distribution at the walls of the hole.

Wanget. al. [14] experimented laser drilling of stainless steel using two closely conjoint pulses with 21ns pulse duration and about 52ns interpulse separation. The experimental results show that the double-pulse drilling rates are higher with more than one order of magnitude than that of conventional single-pulse drilling in air.

A recent research by Yang et. al. [15] to model the melt Flow and heat transfer in laser drilling of super alloys,they formulated a series of differential equations that describe the process from pre-heating to melting and evaporation. The boundary layer theory and integral methods were used to solve Navier-Stokes equation for the melt flow. The numerical results proved that melt flow effect on material removal might be ignored in some cases.

The present research is to investigate; firstly, the performance of material removal during percussion hole drilling in 1.2mm thick stainless steel sheet, using millisecond pulses from flash lamp pumped Nd:YAG laser, via both experiments and theoretical simulation. Secondly, to investigate the thermal history during the heating and the cooling cycles, and to evaluate the effect of the residual heat from one heating pulse on the subsequent one.

2. Experimental Procedure

Percussion laser hole drilling experiments have been conducted using a pulsed Nd:YAG laser provided with an optical fibre as laser energy transmission device and a processing head equipped with a positive focusing lens. The operating specifications of the laser processing system are listed in table 1.The laser spot diameter at the focal plane has been determined by drilling holes in 0.05mm thick stainless steel foil, to assure a negligible transverse heat conduction for its low thermal conductivity, it was in the range of 0.5-0.55mm. This size of laser spot would result in power intensity in the order of $10^9 W/m^2$ (i.e. $10^5 W/cm^{2)}$ for a "Joule/ms" regime of pulse parameters, which indicates no possibility of plasma formation on a metal surface during the processing [3],[4]. A flash lamp Nd:YAG laser with such a spot diameter, shall suggest a high order transverse mode structure of the laser beam, consequently, a uniform intensity profile is assumed across the beam cross section.

Table 1: Specifications of the Nd:YAG laser [16]

Make and type	*TRUMPF, TruPulse 21*
Wavelength	1064 nm
Maximum average power	20 W
Minimum pulse power	100 W
Maximum pulse power	1500 W
Minimum pulse duration	0.2 ms
Maximum pulse duration	50 ms
Maximum pulse energy	15 J
Maximum pulse repetition frequency	900 Hz
Beam parameter product	4 mm.mrad
Core diameter of the light cable	100 µm
Lens Focal length of the processing head	100 mm

Samples of 1.2mm thick sheet of AISI304 stainless steel were used for these experiments, the relevant thermophysical properties of the test material are listed in table 2. Drilling experiments using laser pulses of 1.0 to 7.0ms duration, 0.35 to 2.5J energy as single shots, in addition to a series of 10 pulses of 1ms at 10prf have been performed in ambient air. Tabulation of the experimental settings will be included within the experimental results. It is worthwhile to mention that many experiments have resulted in blind holes, either because of lack of pulse duration and energy, or because of melt recast in the lower crater of the hole.

Table 2: Thermophysicalproperties of AISI 304 stainless steel test material [17, *]

Property	*Min. Value*	*Max. Value*	*units*
Composition (% weight)	C<0.08, Cr=17.5-20, Ni=8-11Mn<2, Si<1, P<0.045, S<0.03, Fe=Balance		
Density	7850	8060	kg/m^3
Tensile Strength	510	620	MPa
Specific Heat	490	530	J/kg.K
Thermal conductivity	14	17	W/m.K
Melting Point	1400	1450	°C
Latent Heat of Fusion	260	285	kJ/kg
Boiling Point [*]	3400	3400	°C
Latent Heat of Vaporization [*]	6500	6500	kJ/kg
[*]: *These properties are unavailable in literature, they have been estimated from alloy composition, with safety margin for the computation purposes.*			

The processed samples were tested and photographed using an optical microscope to determine the hole diameter, the hole depth and the geometrical features generated by the process of hole formation. Magnification factors of 30 or 60 were used for measurements and the photography, as appropriate.

The results of drilling experiments were used to determine the propagation velocity of the heat source into the material, which is fed back to the simulation program. Also, they were for the comparative verification of the simulation results.

3. Simulation in COMSOL

The simulation of the selected drilling cases for either of the heating and the cooling cycles have been performed using "COMSOL Multiphysics 5.1" software. This software provides a programming environment with built-in physical models in the form of differential equations, solving facilities including mesh generation, adaptive mesh refinement, multi-step solutions, phase change, boundaries, initial conditions,….etc. Two-Dimensional Axisymmetric, time dependent model is used for the current simulations as the drilled hole is radially symmetric. The basic geometry is 1.2mm height, a similar dimension is given the radius extent for depicting a semi-infinite slab in the X-Y plane.

3.1 Simulation of the heating cycles

Heating cycles by laser pulses corresponding to selected samples of those which were experimented have been simulated using the conditions and assumptions closest to the real life. Two hole drilling cases have been processed, the heating cycles of the 10prf shots, and the 5.0ms single shot. The basic process parameters are tabulated within the application programs along with the power intensity calculation form. Material properties are also fed assuming initial surface reflectivity as 80%, which is reduced with temperature rise [1, 3]. Therefore, a time-dependent step function is applied to the net absorbed heat flux, assuming reflectivity falls down to 50% when melting starts [3], as shown in figure 1.

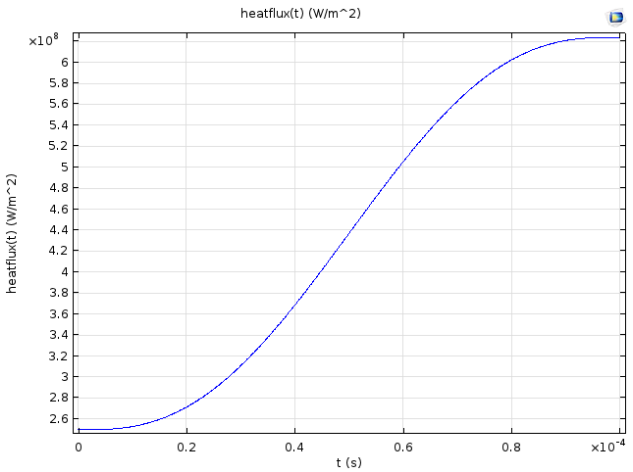

Figure 1: Net heat flux evolution with heating time

The specific heat capacity, *Cp*, also changes considerably during the phase change transition. The difference in specific heat before and after transition can be approximated by, $\Delta Cp = \Delta H / T$, where ΔH is the change in Enthalpy (i.e., latent heat of fusion or vaporization) and $T$is the melting or vaporization point, as applicable [2].

The built-in heat transfer with phase change model has been used which includes modification of the relevant thermophysical properties, besides the capability of introducing heat source motion as velocity in either or both dimensions. This motion ability has been included in the negative Z-directionof the simulation of the 5.0ms single shot only.

Thermal losses due to convection and radiation have been assigned to the high temperature boundaries only, as other boundaries would induce insignificantlosses. The built-in laminar fluid flow facility has also been embedded within the model to characterize the molten and evaporated layers. Mapped type meshes have been employed, which saves computation cost, along with automatic adaptive mesh refinement which is controlled by the physics necessity to refine the solution accuracy. Examples of mapped mesh and adaptive refinement are shown in figure 2.

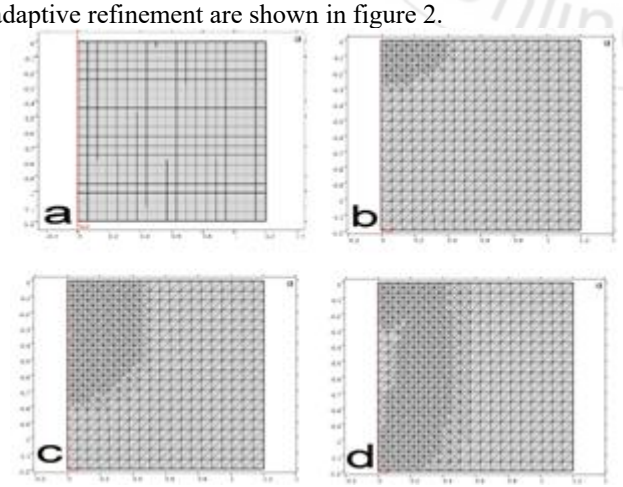

Figure 2: Examples of mapped mesh, a) initial at 0.0ms, b) refined mesh at 0.5ms heating time, c) refined mesh at 2.5ms, and d) refined mesh at 5.0ms.

The 10prf laser drilling shots have been simulated using 10 application modules, each one represents a single 1.0ms, 0.35J pulse. The hole geometry generated from the preceding shot is reproduced at the subsequent application. The boundaries of the heat source, the convection and radiation losses are modified accordingly. As the hole gets deeper, the side wall slope increases and its reflectivity rises, to the extent that a negligible energy proportion would be absorbed by this wall, and the majority of the energy is deposited at the bottom of the hole crater.

The 5.0ms, 2.0J drilling shot has also been simulated using only one application that covers the heating time and similar settings, with one exception that is that is to include propagation speed of the heat source against the material (negative Z-direction). This is to represent the penetration of the evaporation/melting front into the material. A speed value of 0.26m/s has specified which was determined as the mean of the experimental and the 1.0ms simulation results.

3.2. Simulation of the cooling cycles

It has been realized that simulating the cooling cycle which follows the drilling shots is necessary to be considered. This is particularly important for the series of the 1.0ms pulses, to appraise the impact of the residual heat from one pulse on the subsequent one.

A simplified technique was devised, that is to consider the melt layer generated from the former pulse as the ligament thatincorporates the major proportion of the energy left in the process zone. While the other portion of the pulse energy is consumed in the evaporation process. It has been envisaged also, that there is no point of considering the exact thermal gradient in this layer (which ranges from the melting to the evaporation point limits), as this would cost computing with a minor benefit of accuracy. Therefore, the molten layer geometry is passed over to the cooling module as a continuum at a temperature which is the Root Mean Square of the two said above thermal limits. A root mean square method is adopted rather than the direct average, as it is describing a quantum of energy contained within an area.

Three cases have been elected for this simulation, two of them for the 10prf shots, namely after the 4^{th} and the 9^{th} drilling pulses, the third case to represent the cooling after the 5.0ms drilling shot. The 4^{th} shot has been selected as it represent the mid-time process, while the 9^{th} represents the one before the final.

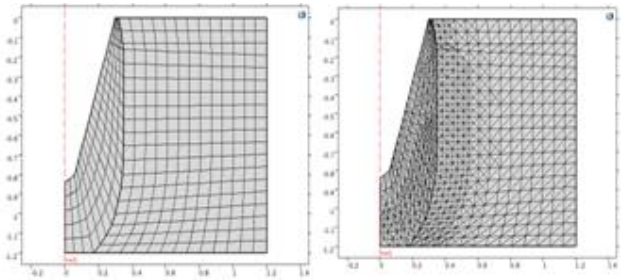

Figure 3: Examples of mapped mesh for the cooling cycles after the 5.0ms shot, left is the initial mesh, right is refined mesh at 1.0ms cooling time.

Heat transfer with phase change model has also been adopted for this procedure, and of course, no heat source is included. Convection and radiation losses are specified for the hot boundaries, whereas the remainder boundaries are considered at room temperature.Mapped mesh type with adaptive refinement were also employed for this simulation, examples are shown in figure 3.

4. Experimental Results and Discussions

A number of drilling experiments, both as single or multiple shots, have been performed for the objectives stated before.Representative results of the microscopical measurements are tabulated in table 3.

Table 3: Measurement results of the drilled holes

Process parameters	Hole diam. (mm)	Hole depth (mm)	Comments and observations
1.0ms,0.7J Single	0.6	0.09	
1.0ms,1.0J single	0.6	0.11	
1.0ms,1.5J single	0.7	0.33	
3.0ms,1.5J single	0.7	0.32	
5.0ms,2.0J single	0.7	through	Blind hole, recast at hole bottom
7.0ms,2.5J single	0.8	through	Blind hole, recast at hole bottom
1.0ms,0.5J 2 prf	0.6	0.85	
1.0ms,0.45J 4prf	0.6	0.1	
1.0ms,0.4J 6prf	0.6	0.21	
1.0ms, 0.35J 7 prf	0.6	0.3	
1.0ms, 0.35J 10 prf	0.6	through	Blind hole, recast at hole bottom

It can be concluded from table 3 that single shots of longer pulses are more efficient in material removal than multiple shots of shorter pulses. This is evident from the result of 5.0ms,2.0J, single shot and that of 1.0ms,0.35J, 10prf. Both cases produced through hole with heavy recast at the hole bottom, yet the difference in energy is 75% (based on the 2.0J value). This can be attributed to the energy lost by the cooling and the resolidification of melt layers during the intervals between the heating pulses.

Sample photographs of drilled holes are shown in figure 4. As can be inferred from this figure, the common features amongst the shown holes geometry are; i) the stepped rings shape of the hole side wall, ii) metal recast on the top edge of the hole and iii) the marks of the liquid metal expulsion in the form of ejection chutes.

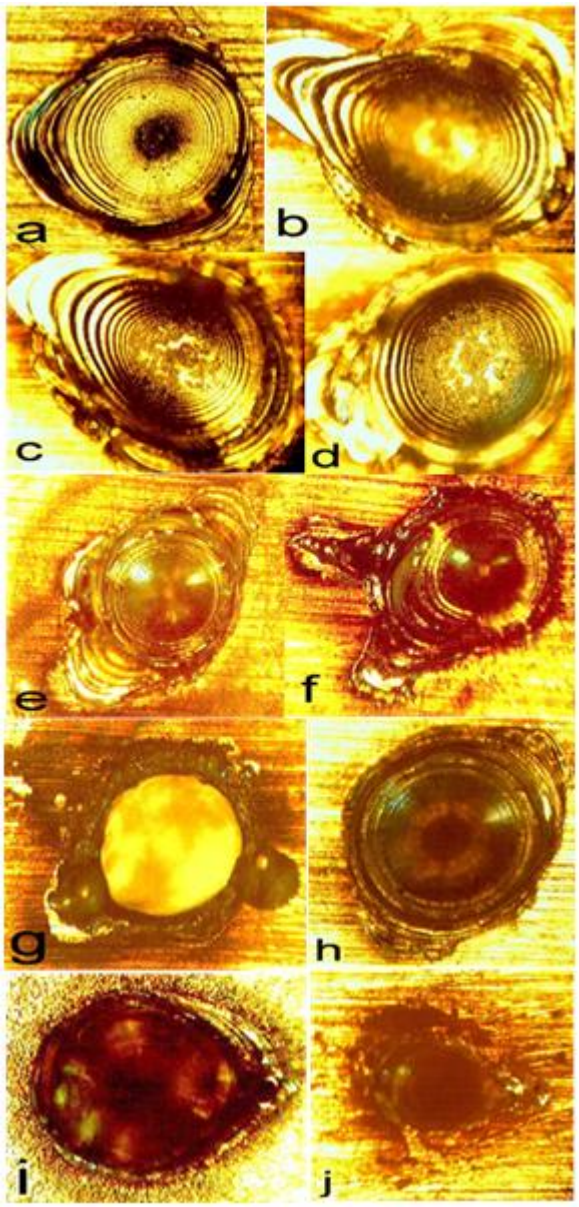

Figure 4: Microscopic photographs at; a) 1.0ms,0.7J, single pulse, b) 1.0ms,0.5J, 2prf, c) 1.0ms, 0.5J, 3prf, d) 1.0ms,0.45J, 4prf, e) 1.0ms,0.4J, 6prf, f) 1.0ms,0.35J, 7prf, g) 1.0ms,0.35J, 10prf, h) 5.0ms, 2.0J, single pulse, i) 3.0ms,1.5J, single pulse, and j)7.0ms,2.5J, single pulse, rear surface.

The stepped ring formation is due to the radial and the upward liquid motion along the side wall which are induced by the vapour pressure when it exceeds the surface tension of the molten layer [2], [4]. The metal recast and ejection chutes (ii and iii) prove that a heavy melt expulsion has occurred. References [2] and [4] states that about 60% of the material is removed by this mechanism. But as the hole gets deeper, it becomes harder to throw up the molten particles, despite the considerable thickness of melt layer, as more kinetic energy is needed to overcome the surface tension. This can be noticed in table 3, as smaller variation in hole depth occurs with increased energy, time or number of pulses.

Photographs (b and c) in figure 4 show extended melt ejection chutes, while (d-g) show multiple chutes, i.e., chute evolution and multiplication is emerge with increased

number of pulses. On the other hand, photographs (h and i) revealthe least metal recast on the hole edge at the top surface, and better results of hole depth compared with the multi-pulse drilling in terms of total energy deposition. Photograph (j) represents the hole exit at the rear surface which approximately 0.3mm diameter, blocked with resolidified metal, and bound with metal recast.

5. Simulation Results and Discussions

This section presents the results of the simulation procedures mentioned in section **3,** including; thermal profiles, thermal gradients and fractions of phases, along with the related discussions.

5.1. Results of multi-pulse heating cycles

Thermal profiles generated by the 10prf heating shotswhich are adapted to show craters resulted due to material removal by evaporation and the molten layers,are shown in figure 5 below. This adaptation is based upon the limits of evaporation and melting points.

The general trends in this figure are; i) almost equal depths by evaporation have resulted from all pulses, ii) the molten layers get thinner with the order of the pulse except the last one, as more energy is deposited at the hole bottom caused by laser rays reflection pattern from the side wall, and iii) as the hole enlarges in depth and diameter, the upper part of the side wall receives less heating energy, this is surely due to high reflection as the laser rays are incident

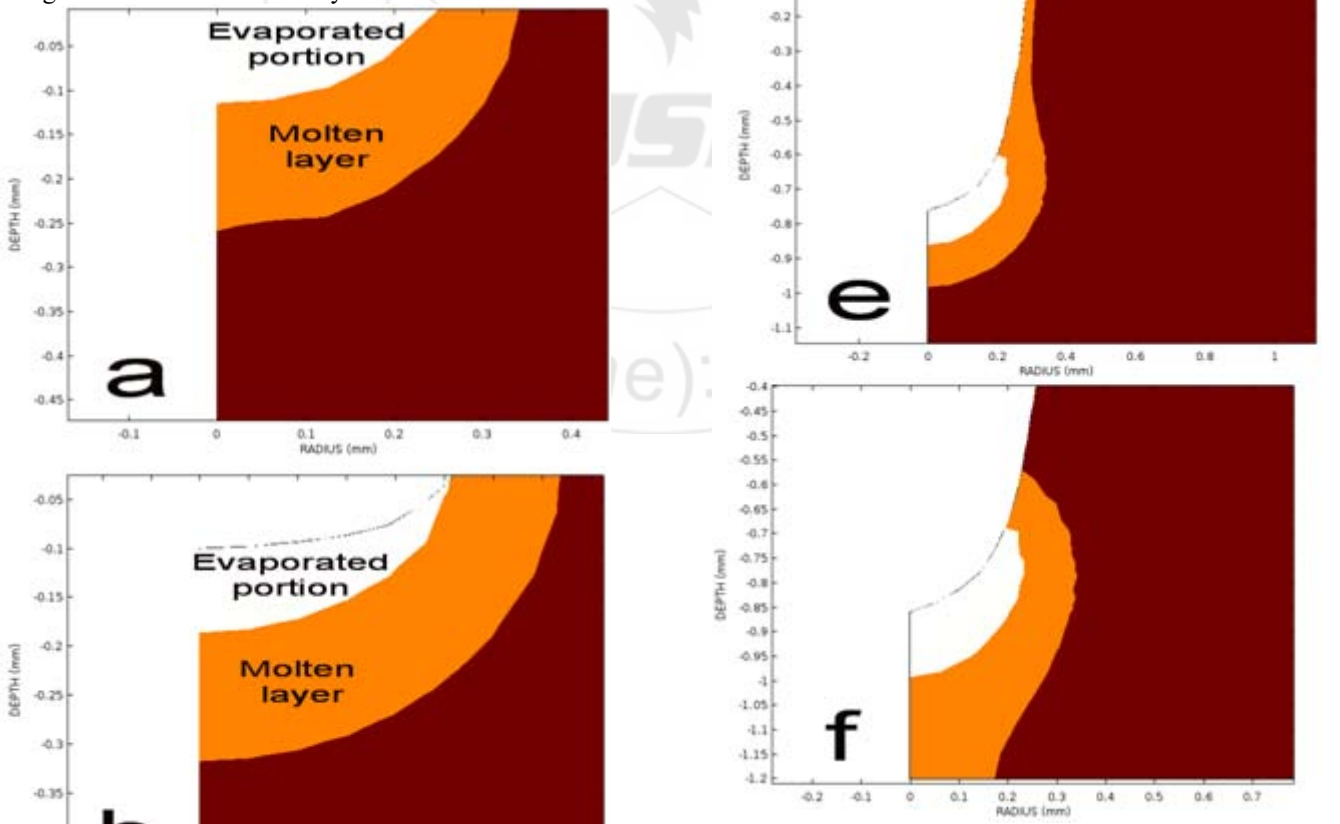

Figure 5: Hole evolution for the 10prf shots, showing the melted and evaporated proportions at the end of; a) 1st pulse, b) 2nd pulse, c) 4th pulse, d) 7th pulse, e) 9th pulse, and f) 10th pulse.

on this part at a grazing angle that does not allow for significant absorption. Although the evaporated craters are forming the stepped bowel shapes shown in figure 5, yet this phenomenon can be strongly overruled by the surface tension and the motion of the liquid metal (see section **4**).

Figure 6illustrates typical examples of the thermal profile (a),thermal gradient (b) and the conductive heat flux (c) at the end of the second pulse. It can be noticed from this figure that imaginary thermal levels are included which are higher than evaporation temperature.

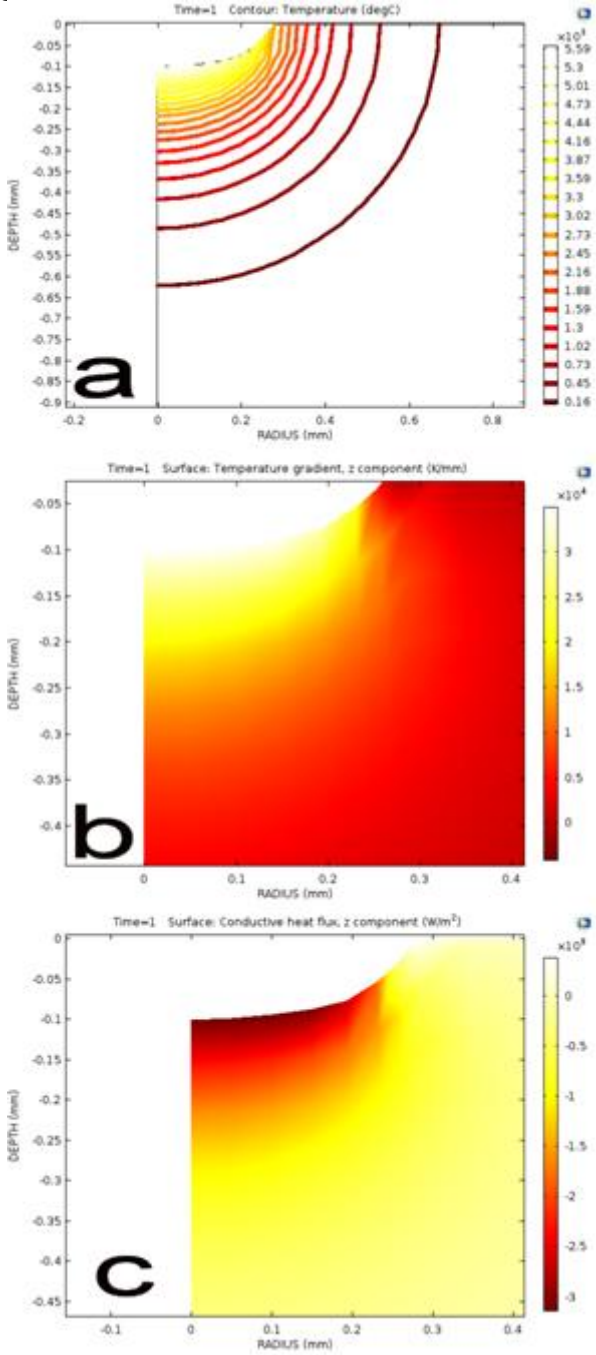

Figure 6: Thermal profile contour lines (a), thermal gradient (b), and the conductive heat flux (c), at the end of the 2nd pulse.

The loci of these contours are considered collectively to constitute the evaporated portion of the metal. The result of the thermal gradient indicates a sharp temperature gradient, in excess of 10000K/mm, close to the melt pool (excluding evaporated and melted layers). This should be considered as a normal range for stainless steel which is characterized by a low thermal conductivity amongst metals.

Relatively higher temperatures and sharper gradients were noticed at the subsequent pulses. The conductive heat flux is negative following Fourier's law of heat transfer, and its peak value is almost of the sameorder as the supplied flux from the laser source.

5.2. Results of the 5.0ms single heating pulse

The thermal profile produced by the 5.0ms,2.0J heating shot is shown in figure 7. This profile has been adapted to show the phase fractions of the vapour, molten layer and the solid stainless steel at the end of this pulse. The coloured part of the figure represents the molten layer, whereas the white area to the left depicts the evaporated portion. The molten layer is quite thick compared with the 1.0ms shots and extending to the rear face, it is shown sectored to reveal the thermal gradient within this zone. The evaporation crater looks conical, and is similar to that produced experimentally.

This profile has been computed using a heat source penetration velocity which would compromise between the experimental observation, the first instances of the heating pulse simulation and the heat balance calculation (taking into account material removal by melt ejection).

The profile of the convective heat flux within the material is shown in figure 8, it is quite noticeable in comparison with that of the 1.0ms shots (which are not shown as they are insignificant). This is obviously due the large molten layer thickness induced by this process.

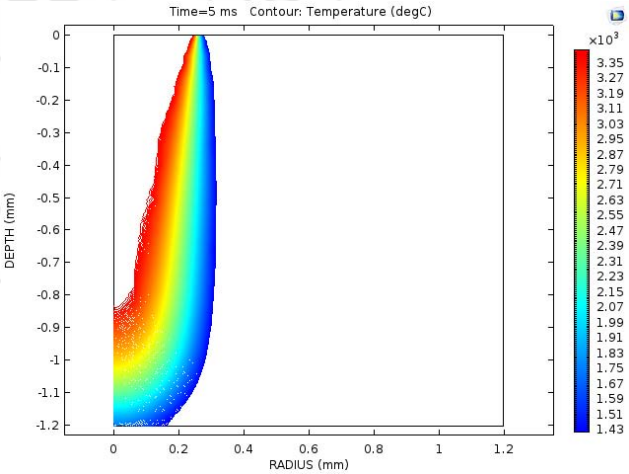

Figure 7: Phase fractions and thermal profile at the end of the 5.0ms drilling pulse.

5.3. Results of the cooling simulation

Three cooling down cases following the 4th, the 9th and the 5.0ms heating pulses, have been simulated on the bases stated in section (**3.2).**

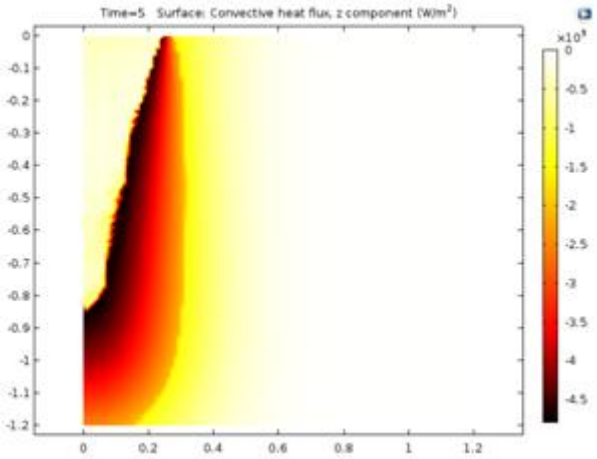

Figure 8: Convective heat flux by the end of the 5.0ms drilling pulse

Figure 9 illustrates the thermal profile contours induced after the 4th pulse, taken at 3.0ms and 30.0ms of the cooling time. This figure indicates two conclusions, a sharp thermal gradient over short distances and a fast cooling time. It can be noticed that it takes 3.0ms only to drop the peak temperature from 2860 to 1550°C, and a period of slightly greater than 30.0ms is good enough to diffuse the heat content of the process zone.

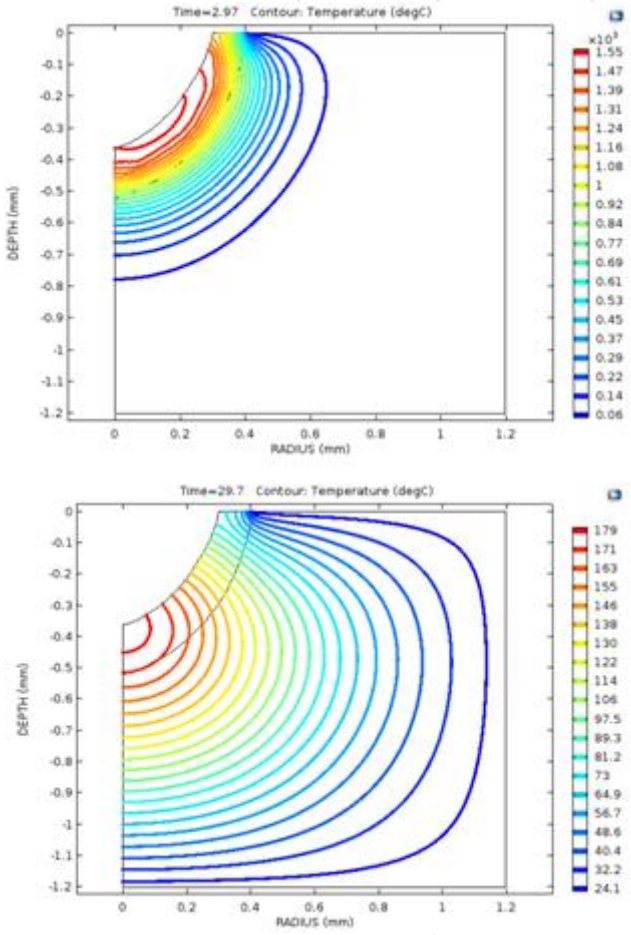

Figure 9: Thermal profile after the 4th pulse at 3.0ms (upper) and 30.0ms (lower) cooling time.

The profiles following the 9th pulse are illustrated in figure 10. A similar behaviors have been noticed with these results, except that marginal difference has occurred with the cooling rate, ashigher ranges of temperature have been resulted from similar periods of cooling time. The reasons for this difference could be; more energy deposition at the hole bottom due to the pattern of laser beam reflection inside the hole, and reduced convection and radiation losses from the hot boundaries as these have sunkinside the hole.

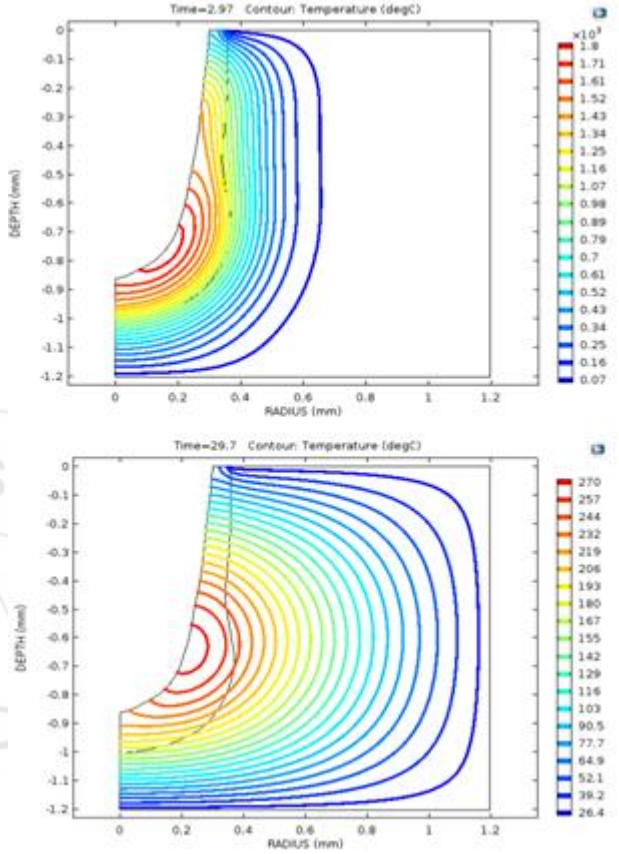

Figure 10: Thermal profile after the 9th pulse at 3.0ms (upper) and 30.0ms (lower) cooling time

Reduced cooling rate has been indicated for the cooling cycle after the 5.0ms drilling shot as can be inferred from figure 11. Higher ranges of temperature have been resulted from almost similar periods of cooling time, which has been resulted from higher energy storage from larger molten volume.

The results of cooling simulation are generally indicating that heat accumulation effect from consecutive pulses is negligible for the ranges of energy, pulse duration and pulse repetition frequency of those considered in this work.

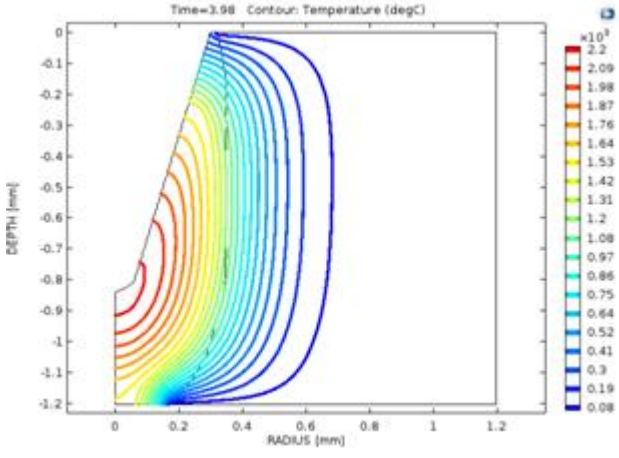

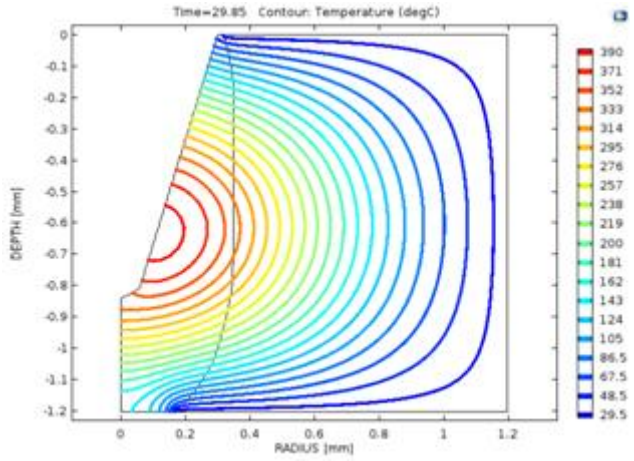

Figure 11: Thermal profile after the 5.0ms pulse at 4.0ms (upper) and 30.0ms (lower) cooling time.

6. Conclusions

The experimental and the simulation procedures which have been performed by the present work may lead to the conclusions that; single shot 2.0J drilling performance was almost the same as the 3.5J (10*0.35) 10prf performance. It can be concluded that for long pulse (i.e. ms) drilling regimes, a continuous long pulse is more efficient than consecutive shorter pulses.

The simulation results presented in COMSOL environment put up a consistent means for the understanding and the prediction of the thermal history during the heating and the cooling sequences

This simulation depicted that full cooling can be realized within a few tens of milliseconds after laser pulse extinguishment, i.e. no residual heat would be carried forward to the subsequent heating pulse when operating with low pulse repetition rate.

References

[1] W. W. Duley, "Laser Processingand Analysis of Materials", Plenum Press, 1983.
[2] W. M. Steen, "Laser material Processing" 3rd edition, Springer, 2003.
[3] J.F. Ready, "Laser Industrial Applications", Academic Press, 1997.
[4] M. von Allmen and A. Blatter, "Laser Beam Interactions with Materials, Physical Principles and Applications", 2nd edition, Springer, 1995.
[5] S. Bandyopadhyay, H. Gokhale, J.K.S. Sundar, G. Sundararajan and S.V. Joshi, "A Statistical Approach to Determine Process Parameter Impact in Nd:YAG Laser Drilling of IN718 and Ti-6Al-4V Sheets", Optics and Lasers in engineering, vol.43, issue 2, Feb 2005,pp163-182.
[6] S. Lazare and V. Tokarev, "Recent Experimental and Theoretical Advances in Microdrilling of Polymers with Ultraviolet Laser Beams", Proceedings of SPIE Vol. 5662, 2004, P.P. 221-231.
[7] J. J. Bornheim, "An Investigation of Laser Drilling Variation and the Application of a Knowledge Management Framework", M.Sc. thesis, Massachusetts Institute of Technology, 2001.
[8] K. Leitza, B. Redlingshöfera, Y. Regc, A. Ottoa and M. Schmidt, "Metal Ablation with Short and Ultrashort Laser Pulses", LiM 2011, Physics Procedia, Vol.12, 2011, P.P. 230–238.
[9] S. Mishra and V. Yadava, "Modeling And Optimization Of Laser Beam Percussion Drilling Of Nickel-Based Superalloy Sheet Using Nd:YAG Laser", Optics and Lasers In Engineering, Volume 51, Issue6, June 2013, P.P. 681-695.
[10] D.K.Y. Low, L. Li andP.J. Byrd, "The Influence Of Temporal Pulse Train Modulation During Laser Percussion Drilling", Optics And Lasers In Engineering, Volume 35, Issue 3, march2001, P.P. 149-164.
[11] S. Döringa, T. Ullspergera, F. Heislera, S. Richtera, A. Tünnermanna and S. Noltea, "Hole formation process in ultrashort pulse laser percussion drilling" LiM 2013, Physics Procedia Vol. 41, 2013, P.P. 431– 440.
[12] G.K.L Ng, and L. Li, "Repeatability characteristics of laser percussion drilling of stainless-steel sheets", Optics and Lasers in Engineering, Volume 39, Issue 1, January 2003, P.P. 25-33.
[13] M. Brajdic, K. Walther andU. Eppelt, "Analysis Of Laser Drilled Deep Holes In Stainless Steel By Superposed Pulsed Nd:YAG Laser Radiation", Optics and Lasers in Engineering, Volume 46, issue 9, September 2008, P.P. 648-655.
[14] X.D. Wang, A. Michalowski, D. Walter, S. Sommer, M. Kraus, J.S. Liu andF. Dausinger, "Laser drilling of stainless steel with nanosecond double-pulse", Optics & Laser Technology, Volume 41, issue 2, March 2009, P.P. 148–153.
[15] Y. Yang, Z. Chen, and Y. Zhang, "Melt flow and heat transfer in laser drilling", International Journal of Thermal Sciences, Volume 107, September 2016, P.P. 141–152.
[16] Anon, "TRUMPF, TruPulse 21 User Manual", TRUMPF Gruppe.
[17] Anon, "Grade 304 Stainless Steel" AZO MATERIALS, an AZoNetwork Site.web page@ AZoM.com.

Author Profile

Mohammed A. Hussain received his B.Sc. in Mechanical Engineering from the University of Baghdad in 1976, M.Sc. in Advanced Manufacturing Technology form the Cranfield Institute of Technology/UK in 1986, and Ph.D. in Laser Based Manufacture from Glasgow University/UK in 1989. He joined Alnahrain University in 1997, where he headed the Department of Laser and Optoelectronics Engineering twice, andstill a staff member in this department.